Restoration of turbulence profile from scintillation indices

A. Tokovinin[1]⋆, V. Kornilov[2]†, N. Shatsky[2]‡, O. Voziakova[2]§

[1]*Cerro Tololo Inter-American Observatory, Casilla 603, La Serena, Chile*
[2]*Sternberg Astronomical Institute, Universitetsky prosp. 13, 119992 Moscow, Russia*

ABSTRACT
An algorithm that permits to measure atmospheric turbulence by statistical analysis of light flux fluctuations in four concentric-ring apertures is described in detail. It consists of computing the scintillation indices for each aperture and pairwise aperture combination and in fitting the set of measured indices to a model with a small number of turbulent layers. The performance of this method is analyzed by means of simulations and using the real data from a Multi-Aperture Scintillation Sensor. It is shown that turbulence profile with a vertical resolution of $\Delta h/h \sim 0.5$ can be reconstructed and that the errors of the measured intensities of turbulent layers are typically around 10% of the integrated intensity. The integral parameters like seeing and isoplanatic angle are measured with few percent accuracy.

Key words: atmospheric effects – site testing – instrumentation: adaptive optics.

1 INTRODUCTION

Knowledge of the vertical distribution of optical turbulence in terrestrial atmosphere is essential for understanding the phenomenon of seeing, for selecting good astronomical sites and for predicting performance of various imaging techniques. For example, the size of a field corrected by adaptive optics (both classical and multi-conjugate) depends on turbulence profile (Roddier 1999). If only ground turbulent layer is adaptively corrected, as suggested by Rigaut (2002), the resulting improvement of seeing is also profile-dependent.

Stellar scintillation is a natural way to sense turbulence remotely. It results from the propagation of wave-fronts distorted by turbulent layers: phase perturbations are converted to intensity fluctuations. The amplitude and characteristic size of intensity fluctuations increase with propagation distance. Hence, it is possible to do remote turbulence sounding by scintillation analysis, as suggested by Peskoff (1968).

Existing techniques for turbulence profile (TP) measurement like balloon micro-thermal sounding or remote optical sounding with double stars, SCIDAR (Fuchs et al. 1998), are expensive and not suitable for continuous monitoring. Tokovinin & Kornilov (2002) proposed to obtain low-resolution profiles from the statistical analysis of light fluxes in four concentric-ring apertures. Such Multi-Aperture Scintillation Sensor (MASS) was actually built and tested by Kornilov et al. (2002). Compared to the previous single-star scintillometer of Ochs et al. (1976), MASS has a better vertical resolution of $\Delta h/h \sim 0.5$ and good absolute calibration. This has

been achieved by means of careful signal processing and interpretation. In this paper we describe this algorithm step by step. Although the algorithm was developed for a specific instrument, MASS, it is more general and can be applied to other instruments that would use the same principle.

A simple and robust TP monitor like MASS is of interest for modern site testing and for support of adaptive optics and interferometry operations at the existing observatories. It is being used already to study the statistics of TP at Cerro Tololo (Tokovinin et al. 2003) and La Silla observatories in Chile and at Mauna Kea (Hawaii); more applications are planned in the near future.

The principle of MASS operation is briefly introduced in Sect. 2. Fluctuations of stellar light caused by scintillation are characterized by the *scintillation indices* (SIs) that are computed by the algorithm presented in Sect. 3. Turbulent layers in the atmosphere contribute to a given SI according to the corresponding *weighting function* (WF, Sect.4). Knowing both indices and WFs, we can restore the TP if a simple model of atmosphere with few discrete layers is adopted, as explained in Sect. 5. In Sect. 6 we study the vertical resolution and precision of such a restoration technique and show examples of its application. Alternatively, some atmospheric parameters of interest can be derived directly from SIs without explicit profile restoration (Sect. 7). The conclusions are given in Sect. 8.

2 THE MASS INSTRUMENT

In Fig. 1 the principle of MASS and its data processing are illustrated. Upon propagation through a turbulent layer and further down to the ground, light of a stellar source acquires amplitude and phase fluctuations. Amplitude fluctuations are the cause of scintillation (twinkling) of stars, they resemble a pattern of 'flying shad-

⋆ E-mail: atokovinin@ctio.noao.edu
† E-mail: victor@sai.msu.ru
‡ E-mail: kolja@sai.msu.ru
§ E-mail: ovoz@sai.msu.ru
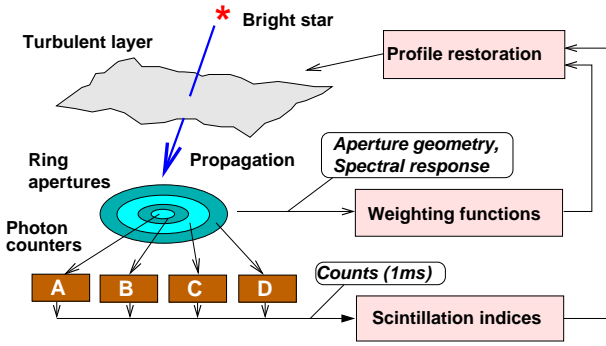
Figure 1. Principle of turbulence profile measurement with MASS.

ows' on the ground. The characteristic size of flying shadows is of the order of Fresnel radius $\sqrt{\lambda z}$ for a propagation distance z and a wavelength λ. Thus, the spatial structure of single-star scintillation contains information on the distance to turbulent layers (Peskoff 1968).

In MASS, the flux of a bright star in four concentric apertures A, B, C, and D is registered. Those apertures together act as a spatial filter. The smallest aperture A has a diameter of 2 cm, it is sensitive to turbulence at altitudes above 0.5 km. The largest aperture D has outer diameter of 13 cm and senses mostly the high layers. Statistical analysis of the scintillation signals in all four apertures permits to localize turbulent layers and to measure their intensities.

The MASS instrument is described by Kornilov et al. (2002). Briefly, it consists of a feeding telescope with a clear (unobstructed) aperture of 14 cm diameter and a detector box. Within the box, image of the exit pupil is segmented into rings by a system of concentric mirrors with different tilts – segmentator. The four beams A, B, C, and D are then directed to the four photomultipliers (PMTs) which work in photon-counting mode with a pulse resolution about 15 ns. The spectral response of MASS is determined by a glass filter which passes the wavelength band from 400 to 550 nm, with a full-width at half maximum (FWHM) bandwidth of 100 nm. A star of B=0 magnitude gives count rate in the smallest A-aperture of about 200 counts per millisecond. The series of photon counts are used to compute the 10 SIs (4 normal and 6 differential) and to restore the TP as explained below.

MASS in its normal mode is not sensitive to the near-ground turbulence because the latter does not produce any scintillation. When a positive lens is placed in the focal plane, the image of a pupil on the segmentator is defocused and corresponds to the additional 'virtual' propagation, following the idea of Generalized SCIDAR (Fuchs et al. 1998). This *generalized* mode permits to detect low-altitude turbulence and thus to measure the total seeing. During acquisition, a lens is placed and removed periodically, so that both normal and 'shifted' indices are accumulated quasi-simultaneously. We use only 3 'shifted' indices from the smallest apertures, extending the set of measured indices from 10 to 13. Additional instrumental effects (diffraction at the entrance pupil, guiding errors, optical aberrations) complicate data acquisition and interpretation in the generalized mode and limit the altitude shift to small values (e.g. 0.5 km). For this reason, we do not use generalized mode with a small feeding telescope.

MASS can be used both with its own feeding telescope and with any other telescope. In the latter case, a 2-lens 'transformer' is placed before the entrance aperture to adapt the instrument to a specific telescope focal length, projecting the segmentator onto the primary mirror with a suitable scale. In cassegrain telescopes with central obscuration the segmentator must be projected off-axis onto clear part of the pupil. If the clear part is much larger than 14 cm, the generalized mode becomes feasible because diffraction and guiding errors are no longer troublesome.

3   SCINTILLATION INDICES AND THEIR ERRORS

In this Section we explain how the series of raw photon counts are processed to get SIs. Suppose that instantaneous light flux received by a given MASS aperture is X. The SI s_x is defined as a variance of flux normalized by the square of average flux:

$$s_x = \overline{(X - \overline{X})^2}/(\overline{X})^2 = \overline{(X/\overline{X})^2} - 1. \tag{1}$$

Differential SI s_{xy} (Tokovinin 1998, 2002) is defined similarly as a variance of the difference of normalized fluxes X and Y in a pair of apertures:

$$s_{xy} = \overline{(X/\overline{X} - Y/\overline{Y})^2} = s_x + s_y - 2\overline{XY}/(\overline{X} \cdot \overline{Y}) + 2. \tag{2}$$

Differential SIs are related to covariances.

The instantaneous fluxes X and Y are not known. Instead, we measure the series of photon counts in the four channels with finite micro-exposure time t. Let x_i and y_i be these counts in two channels, N – the number of samples during 1 s exposure ($N = 1000$ for $t = 1$ ms). To obtain correct SIs from this data, we must take into account the non-linearity of photon counters, subtract contribution of photon noise, and extrapolate the indices to zero exposure time, thus removing the bias caused by finite t. Correction for background (dark count of PMTs and light from the sky) must be made as well. These operations are done in several steps.

Step 1. Compute the mean count values $\overline{x}$ for all channels.

Step 2. Compute the raw auto- and cross-covariances of the counts in all channels. Auto-covariances are needed for time lags of 0, 1, 2 sampling intervals, cross-covariances – only for lags 0 and 1. For any two channels x and y ($x = y$ for auto-covariance) and for time lag k ($k = 0, 1, 2$) the covariance $\rho'_{xy,k}$ is found as

$$\rho'_{xy,k} = \frac{1}{2(N-k)} \sum_{i=1}^{N-k} [(x_i - \overline{x})(y_{i+k} - \overline{y}) + (x_{i+k} - \overline{x})(y_i - \overline{y})]. \tag{3}$$

Step 3. Correct the raw covariances and mean counts (designated here by prime superscript) for the non-linearity of photon counters (Kornilov & Pogrosheva 1989). The non-linearity parameter $L = \tau/t$ is the ratio of counter dead time τ to the micro-exposure time t.

$$\overline{x} = \overline{x}'(1 + L\overline{x}'), \quad \rho_{xy} = \frac{\rho'_{xy}}{(1 - 2L\overline{x}')(1 - 2L\overline{y}')}. \tag{4}$$

Step 4. Compute the SIs that are free of photon noise, corrected for background and extrapolated to zero micro-exposure time (1 ms is not short enough to freeze scintillations in the smallest apertures). The background B_x is the number of background counts in channel x per micro-exposure; it is almost always less than 1% of the signal and not critical for data reduction. The *non-Poisson parameter* p is the ratio of the variance of photon counts to their mean value at constant light, $p = (\overline{x^2} - \overline{x}^2)/\overline{x}$. For an ideal photon counter $p = 1$, but for real PMTs at low fluxes the measured p is typically in the range from 1 to 1.1. The covariances are already corrected for non-linearity at this point. The normal and differential SIs are:

$$s_x = \frac{1.5[\rho_{xx,0} - p\overline{x}] - 0.5\rho_{xx,1}}{(\overline{x} - B_x)^2}, \tag{5}$$

$$s_{xy} = s_x + s_y - 2\frac{1.5\rho_{xy,0} - 0.5\rho_{xy,1}}{(\overline{x} - B_x)(\overline{y} - B_y)}. \tag{6}$$

The derivation of these formulae is given in the Appendix A. The set of 10 SIs is computed every second. Thus, slow flux variations (below 1 Hz) caused by unstable transparency, changing zenith distance, etc. do not contribute to the SIs.

Step 5. Estimate average SIs and their errors from $K = 60$ 1-s measurements accumulated during 1 min. If 1-s measurements were uncorrelated, the error of the mean would be simply $\sqrt{K}$ times less than the rms scatter of the data. Partial correlation of data is taken into account by the following formula for the variance $\sigma_{\overline{s}}^2$ of the average SI $\overline{s}$:

$$\sigma_{\overline{s}}^2 = \frac{1}{K}\left[\rho_{s,0} + 2\sum_{k=1}^{K-1}(1 - k/K)\rho_{s,k}\right], \tag{7}$$

where $\rho_{s,k}$ is the auto-covariance of SI s for the lag k computed by the same formula 3 as used for photon counts. We found that the *relative* errors $\sigma_{\overline{s}}/\overline{s}$ of all normal and differential SIs estimated by the above formula are about 2%, except the smallest differential SI s_{AB} where photon noise is important and the relative error is $3\% - 7\%$, depending on the photon flux. Below we explain why all other SIs have the same relative errors independently of scintillation strength and stellar flux.

The variance of the normalized light intensity from which SI is derived is a sum of scintillation variance s_x and photon noise variance $1/\overline{x}$; the latter is subtracted (Eq. 5), but its statistical uncertainty still contributes to the SI error. The relative proportion of those two terms depends on the photon flux, TP and type of the index considered. For example, 1 ms flux in the smallest aperture A for a 2.5-magnitude star is $\overline{x} = 20$ photons, while typically $s_A \sim 0.1$, making the photon noise contribution unimportant. This applies to other indices as well. Only the differential SI in the smallest aperture pair under good $(0''.5)$ seeing is smaller than the photon noise variance ($s_{AB} \approx 0.006$), explaining why this SI is measured with a larger error.

The contribution of these terms to the error of SI depends also on the correlation time of these signals which is different. It is well known that a signal with a correlation time τ measured during acquisition time T would have a relative error of its variance estimate of $\sqrt{\tau/T} = 0.013$ for $\tau \sim 0.01$ s. The photon noise has a white spectrum, so for a sampling time $t = 1$ ms the relative error of the photon noise variance estimate is only $\sqrt{t/T} = 0.004$, or ~ 3 times less than for the same scintillation signal. In fact turbulence is not quite stationary even during 1 min., increasing the scatter of 1-s SIs and the errors of mean SIs compared to the estimates for a stationary case given above; this is why we rely on the experimental estimates of SI errors.

If the *relative* noise in the measured SIs is more or less constant, the relative noise of TPs restored from this data will also be constant. It means that the sensitivity of MASS improves when turbulence is weak and degrades under strong turbulence, as confirmed below by the analysis of real data.

4 WEIGHTING FUNCTIONS

Atmospheric turbulence can be considered as a collection of independent turbulent layers at altitudes h_i. The intensities of those lay-
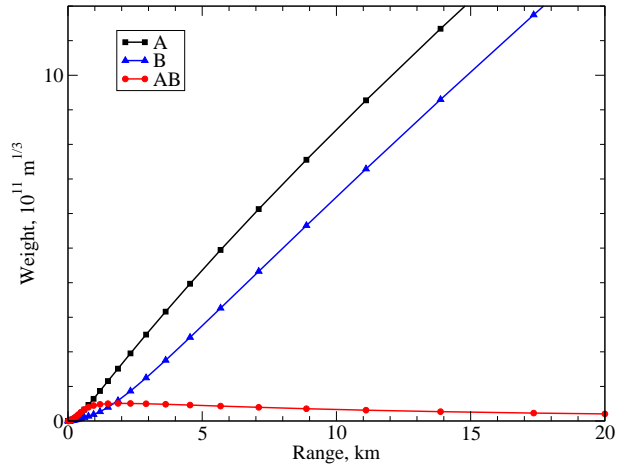
Figure 2. Example of the weighting functions for the two smallest MASS apertures, A and B, computed for the combination of the actual filter bandpass, PMT sensitivity, and spectral energy distribution of a star of spectral type A5.

ers J_i are the integrals of refractive index structure constant $C_n^2(h)$ over the layers

$$J_i = \int_{i-\text{th layer}} C_n^2(h)\mathrm{d}h, \tag{8}$$

they are measured in $\text{m}^{1/3}$. The TP is completely defined by the set of $\{h_i, J_i\}$ values. This might appear different from the classical view of TP as a continuous function $C_n^2(h)$, although it is nothing else but a discrete representation of such function. Optical effect of turbulence is directly related to the intensities J_i rather than to $C_n^2(h)$.

The theory of weak perturbations (Tatarsky 1961; Roddier 1981) establishes a linear relation between some scintillation index s_x and the intensities of all layers:

$$s_x = \sum_{i=1}^{I} J_i \, W_x(h_i \sec\gamma)\sec\gamma, \tag{9}$$

where γ is the zenith distance of a star, $z = h_i \sec\gamma$ is the propagation distance, and the altitudes h_i are counted from the observatory level rather than from sea level. The coefficients $W_x(z)$ are called *weighting functions* (WFs), they depend on wavelength and aperture size. Eq. 9 is valid only for weak (non-saturated) scintillations, which means practically $s_A < 0.3$. Application of the linear theory to saturated scintillations will result in under-estimation of J_i.

The formulae to compute WFs for normal SIs and monochromatic light can be found in many publications. Tokovinin (1998, 2002) gives these formulae for both normal and differential SIs and for apertures of arbitrary shape. However, it turns out that for differential SIs the effect of spectral bandpass is significant and the polychromatic WFs can not be computed as weighted average of monochromatic WFs. Formulae for polychromatic WFs are provided in (Tokovinin 2003) and reproduced in Appendix B for completeness.

Polychromatic WFs computed for the two smallest MASS apertures are plotted in Fig. 2. The MASS bandpass is wide enough, so we have to take into account the variations of energy distribution in the stellar spectrum within the bandpass. Stars are subdivided into 12 groups according to their spectra and the WFs are

pre-computed for each spectral group separately. During observations, an adequate table of WFs is selected depending on the star.

Eq. 9 can be written in a matrix form by considering the vector of indices $\mathbf{S}$ of length $M = 10$ ($M = 13$ in generalized mode), the vector of layer intensities $\mathbf{J}$ of length I and the matrix $\mathbf{W}$ with elements $W_{mi} = W_m(h_i \sec \gamma) \sec \gamma$:

$$\mathbf{S} = \mathbf{W}\mathbf{J}. \tag{10}$$

This formula is the basis of TP restoration.

5 RESTORATION OF TURBULENCE PROFILE

5.1 The model

We measure only a small number of indices, much less than any realistic number of atmospheric layers. However, in order to obtain some information on TP we fit the data (indices) to a *model* with only a few layers. It will be shown that such procedure leads to a low-resolution TP which adequately represents any real TP. The 'layers' restored in this way are in fact thick slabs of turbulence. Despite the crudeness of such model, layer intensities are measured correctly.

Two alternative restoration techniques are used. The first *fixed-layer* method assumes layers at some pre-defined altitudes h_i. In this case the relation between data $\mathbf{S}$ and unknowns $\mathbf{J}$ is linear (Eq. 10). The second *floating-layer* method uses a model with only three layers that can be located at any altitude and solves Eq. 10 for the unknowns h_i, J_i. In both models the number of unknowns must be less than the number of measurements M. In fitting models to the data, we search for model parameters that minimize the χ^2 function. Let $\overline{s}_m$ be the measured average indices, $\sigma_{\overline{s}m}$ – their variances (as estimated from Eq. 7), $\hat{s}_m$ - the expected (or model) indices computed from Eq. 10. Then

$$\chi^2 = \sum_{m=1}^{M} \frac{(\overline{s}_m - \hat{s}_m)^2}{\sigma_{\overline{s}m}^2}. \tag{11}$$

The minimum value of χ^2 is a measure of correspondence between model and data. In theory, its expected value is $M - I$, where I is the number of model parameters. In practice it is almost always larger for many reasons (e.g. inadequate model, biased data). The data (indices) are not mutually independent because 10 SIs are computed from only 4 light fluxes.

Below we consider each restoration method in more detail.

5.2 Fixed-layers restoration

For fixed-altitude layers the system (10) is linear and a solution $\hat{\mathbf{J}}$ that minimizes χ^2 is found by the least-squares method (Press et al. 1992):

$$\hat{\mathbf{J}} = (\mathbf{W}^T\mathbf{W})^{-1}\mathbf{W}\mathbf{S}, \tag{12}$$

where the system matrix $\mathbf{W}$ and the data are re-normalized by the errors, $W_{mi} = W_{mi}/\sigma_{\overline{s}m}^2$ and $S_m = \overline{s}_m/\sigma_{\overline{s}m}^2$.

The noise variance of the i-th restored layer intensity σ_{Ji}^2 is then equal to the i-th diagonal element of the inverse normal matrix:

$$\sigma_{Ji}^2 = (\mathbf{W}^T\mathbf{W})_{ii}^{-1}. \tag{13}$$

Given that the least-squares method is not quite applicable in our case (correlated data, non-negativity constraint), Eq. 13 can be used only for a rough estimate of the resulting errors.

It is well known that the normal matrix of the least-squares problem can be ill-conditioned. This happens when two or more unknowns have similar influence on the data. For example, if we select two pre-defined layers at 10 and 11 km, the WFs for these layers will be very similar, hence the matrix $\mathbf{W}$ will be almost degenerate. Reasonable choice of layer altitudes is essential for successful restoration. We have chosen a logarithmic altitude grid (1, 2, 4, 8, 16 km) that matches the character of WFs. A 6-th layer at 0.5 km was added after it became clear that it was required to model data in some cases. A layer at 0 km is added in the generalized mode. On the other hand, if model contains too few layers the fit to the data will be poor (large χ^2).

Linear restoration does not take into account the fact that layer intensities J_i must be non-negative. So, instead of solving (10) by least squares, we minimize χ^2 (Eq. 11) directly with this additional constraint. Technically, we change variables to $J_i = y_i^2$ and minimize χ^2 over y_i using the standard Powell method.

5.3 Floating-layers restoration

The second restoration method uses a model with only three layers and 6 parameters $\{h_i, J_i\}$. Real TPs often contain strong layers which can be localized with this technique. Of course, the continuously-distributed turbulence that is also always present in the atmosphere is included into the 3 layers as well.

The implementation of floating-layer method is more complicated and computer-intensive than for fixed layers. The problem is highly non-linear, so minimization of χ^2 by gradient techniques leads to local minima. Instead, we check all plausible combinations of altitudes and for each combination find the best-fitting layer intensities and the corresponding χ^2. The altitude of the lowest layer h_1 is selected among the grid points (with logarithmically-uniform step). For each h_1, the altitude h_2 is selected from the same grid to be larger than h_1, then h_3 is selected larger than h_2. This process eliminates duplicate computation. For each altitude combination $\{h_i\}$ layer intensities are found by direct inversion of the linear Eq. 10 (the matrix $\mathbf{W}$ is in fact inverted by singular-value decomposition). Negative J_i that may result from this procedure are set to zero, and the χ^2 that corresponds to the given $\{h_i\}$ is finally computed. When all altitude combinations are checked, the one with minimum χ^2 is taken as a solution. Floating-layer restoration takes less than 1 s on a modern PC computer.

5.4 Example of profile restoration

The example of application of both methods to real data is shown in Fig. 3, see also (Kornilov et al. 2002). The consistency between successive profiles is immediately seen – a convincing evidence that restoration is indeed successful. The changing character of turbulence is apparent: after 3h UT, the floating-layer method does not give consistent layer altitudes, indicating that turbulence is likely to be distributed continuously. The two restoration methods are complementary to each other.

The residuals of three representative SIs to fixed-layer model are plotted in Fig. 4 for the same data. It is typical that relative residuals are under 5% most of the time. Some systematic deviations from zero (few percent) are observed in s_D, signaling that the actual structure of high-altitude turbulence is not perfectly represented by our simple model. The residuals to floating-layer model are quite similar. Low residuals translate to low χ^2/N, typically under 10.
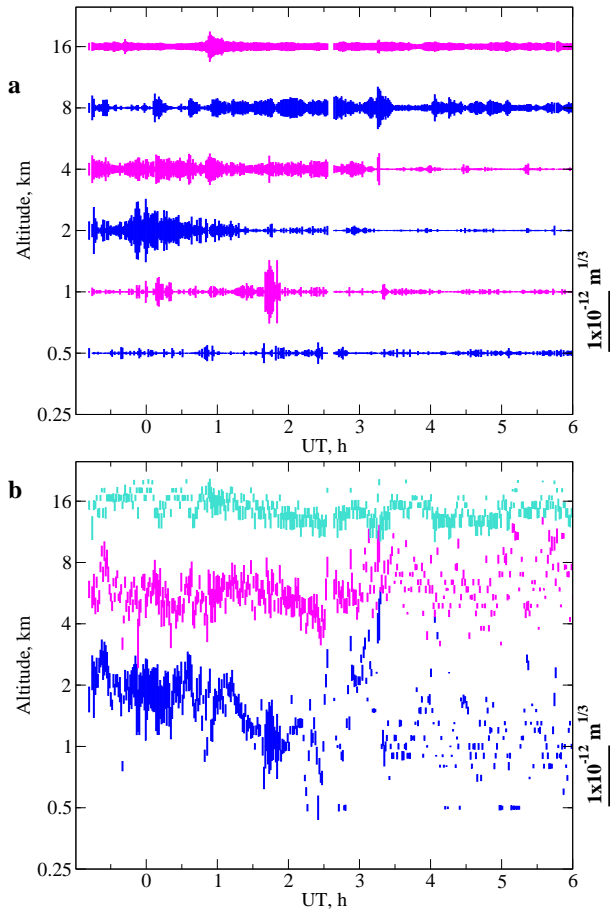
Figure 3. Turbulence profile evolution during several hours on September 11/12 2002 as measured with MASS at Cerro Tololo (Chile). **a** – fixed-layer method, **b** – floating-layer method. Length of bars is proportional to the intensities of turbulent layers with the scale indicated on the right.
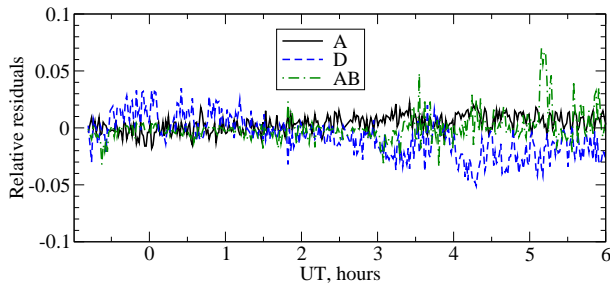

Figure 4. Relative residuals (observed minus modeled divided by modeled) of scintillation indices in apertures A, D, and AB for the data in Fig. 3, fixed layers restoration.

6 PERFORMANCE OF FIXED-LAYER RESTORATION

6.1 Numerical modeling: one and two layers

The fixed-layer restoration was studied by numerical simulations. For some input TP, we computed true SIs, added a realistic noise (2% relative for all SIs, 4% for s_{AB}) and restored the TP by fixed-layers method. Our simulations assume independent noise on all SIs which is only an approximation.

First, we simulated restoration of a single layer located at different altitudes. For each layer altitude, independent noise realiza-
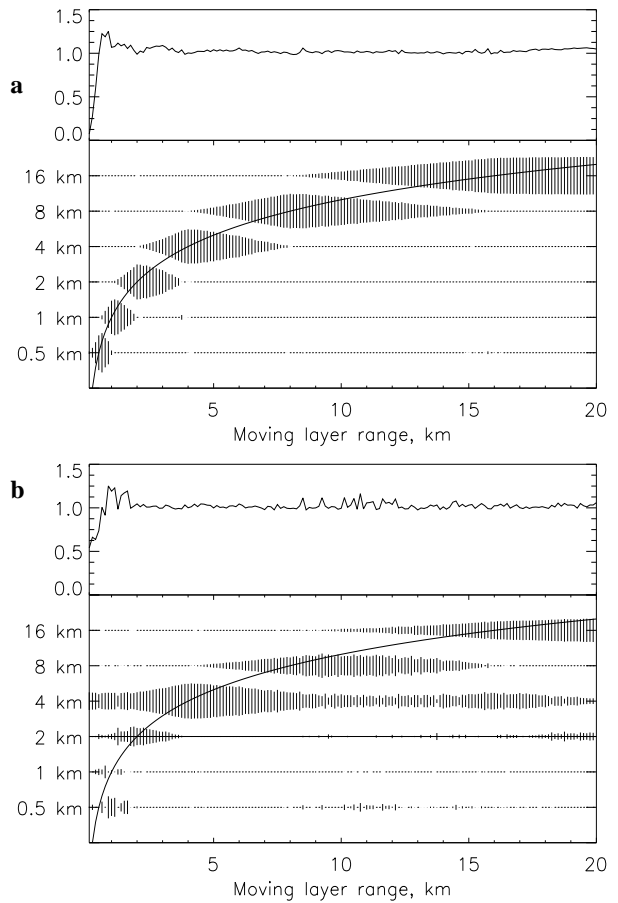

Figure 5. a – simulation of the response of the fixed-layers restoration to a single turbulent layer located at different altitudes (horizontal axis). The length of bars shows the reaction of slabs in relative units. The upper curve shows the sum of all reactions. **b** – same for two equal layers, one moving and another fixed at 4 km.

tions were added to the scintillation indices, as in real data. When the layer altitude coincides with one of the pre-defined model altitudes h_i, its intensity is retrieved correctly. Otherwise, a layer is re-distributed among the two nearest slabs, but the total intensity of these slabs is again equal to the input layer intensity. In Fig. 5a a reaction of each slab is plotted when a single 'floating' layer changes its altitude. It is seen that response functions of pre-defined slabs are triangular. The sum of response functions is practically constant, which means that the total turbulence intensity (hence free-atmosphere seeing) is measured correctly for all layer altitudes. Noise in the restoration is barely noticeable.

A reaction of MASS to two layers is simulated in Fig. 5b. Here the input TP consists of two equal layers, one fixed at 4 km and another with variable altitude. The overlapping layers are successfully separated, but the noise is more pronounced. However, the noise mostly tends to re-distribute the intensity between adjacent slabs, with less effect on the total intensity.

6.2 Realistic profiles

The fixed-layer restoration procedure was simulated with real turbulence profiles and was shown to give reasonable results (Tokovinin & Kornilov 2002). Here we repeat this exercise with realistic noise levels appropriate for MASS (see above). We use
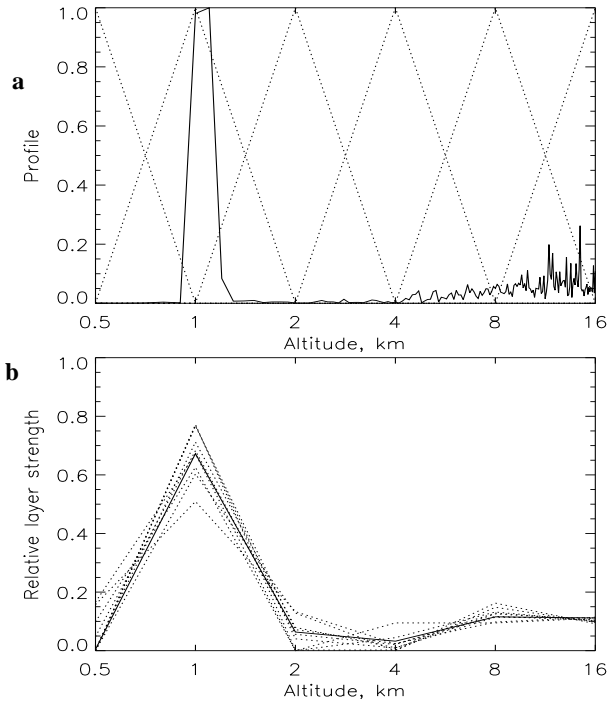
Figure 6. a – The turbulence profile number 50 as measured at Paranal (full line) and the idealized response functions of MASS in relative units (dotted lines). **b** – The results of 10 restorations with independent noise realizations normalized by J_{tot}: the true profile in full line, restored profiles in dotted lines.
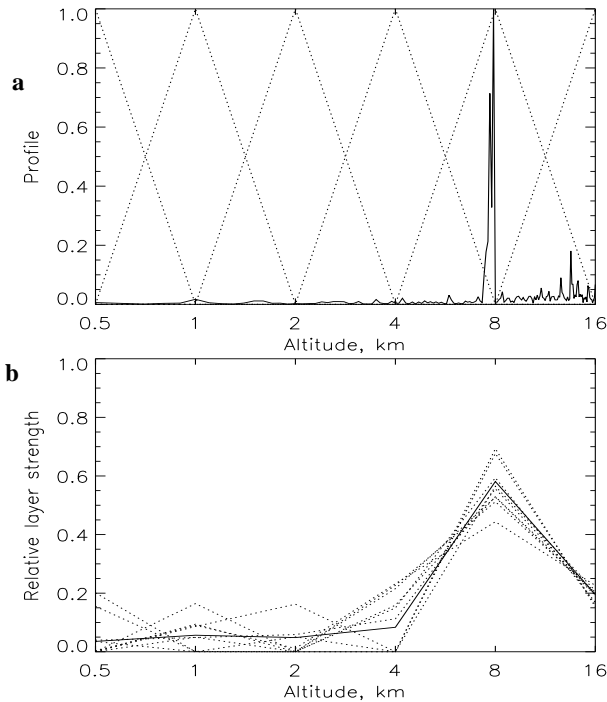
Figure 7. Same as Fig. 6 for Paranal profile number 51.
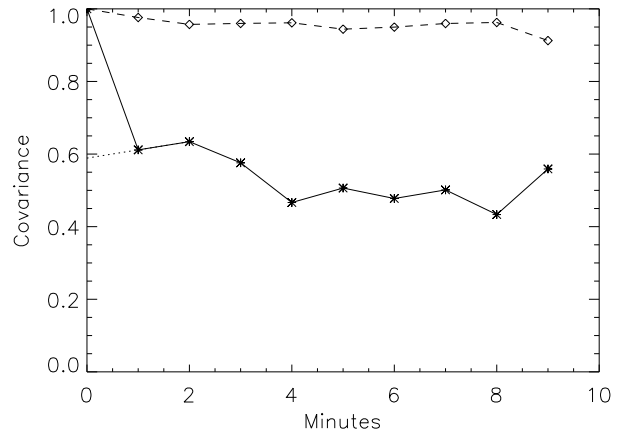
Figure 8. Normalized auto-covariance functions for the 0.5 km (full line and asterisks) and 16 km (dashed line and diamonds) layers for the night of June 19, 2002. The dotted line shows the extrapolation to zero from the first two points.

the same set of 12 real turbulence profiles measured by balloons at Cerro Paranal in Chile during the PARSCA campaigns (Fuchs & Vernin 1993); those profiles are plotted in (Le Louarn et al. 2000).

Figs. 6 and 7 illustrate the results for two very distinct cases. The scintillation indices were computed from real profiles (with 100 m vertical resolution) and artificially corrupted by noise. Then a restoration procedure was applied several times, with different noise realizations. True intensities of the 'layers' were computed by integrating the products of profiles and triangular response functions, to be compared with the results of restoration. Here we address two problems: i) the reaction of the crude 6-layer model to realistic complex profiles and ii) stability of restoration with respect to noise.

The root-mean-square (rms) restoration error was computed for each layer and expressed as a fraction of the total integral J_{tot} (the sum of true layer intensities), because errors in MASS are proportional to the signal. These errors are larger for lower (0.5 and 1 km) layers, reaching 20% in the worst cases and around 10% typically. For the highest 16 km layer the errors are only few percent. The curves in Figs. 6,7 show that the restoration errors mostly consist in re-distributing turbulence between slabs rather than in the estimate of the total intensity. Indeed, the relative rms error of the 'measured' J_{tot} is only from 5% to 10% for all 12 profiles.

6.3 Noise estimates from real data

The performance of fixed-layer restoration was checked on real data by analyzing the reproducibility of the measured profiles. We attempted to separate real variations of the turbulence strength occurring in each slab and the instrumental noise by means of covariance analysis. Let $J(t_i)$ be the strength of some layer (slab) as measured by MASS on moments t_i (with a time resolution of 1 min.). Then the auto-covariance $C_{J,\Delta t}$ is

$$C_{J,\Delta t} = \frac{1}{N} \sum J(t_i)J(t_i + \Delta t), \tag{14}$$

where N is the total number of samples entering into the sum. An example of the auto-covariance is given in Fig. 8.

The idea of noise estimation is to extrapolate C linearly to zero using the first and second points. Then the difference with the actual value will be a rough estimate of the MASS noise variance:

Table 1. Noise of measured layer intensities σ_J in 10^{-13} m$^{1/3}$

Date, 2002	N_{prof}	J_{tot}	Layers, km					
			0.5	1	2	4	8	16
19/06	597	1.0	0.10	0.07	0.13	0.08	0.12	0.04
22/06	473	0.8	0.04	0.07	0.03	0.04	0.05	0.03
10/07	546	3.2	0.14	0.15	0.45	0.17	0.10	0.06
24/07	498	8.3	0.60	0.81	0.36	0.27	-	0.03

$$\sigma_J^2 = C_{J,0} - [2C_{J,1} - C_{J,2}]. \tag{15}$$

It should be stressed that σ_J^2 is actually an *upper limit* for noise because it includes natural short-scale variations of the turbulence intensity.

The results of the calculations are given in Table 1. The nights selected for this analysis are different: the first two had an exceptionally calm upper atmosphere, 10/07/2002 was typical and 24/07/2002 was worse than average. The total number of profiles N_{prof} and the average turbulence integral for each night J_{tot} are given for reference. In one case the extrapolation method failed to give a non-negative noise estimate, which is not surprising for a statistical technique.

The signal-dependent noise characteristics are confirmed by the actual analysis: noise is roughly proportional to J_{tot}. It never exceeds $0.14\ J_{\mathrm{tot}}$, and this is an upper limit because some fast turbulence variations are included. The absolute sensitivity of MASS is impressively high, especially at high altitudes. A noise-equivalent J of $0.03 \cdot 10^{-13}$ m$^{1/3}$ corresponds to a seeing of only $0.''04$. The worst-case error encountered in Table 1 is $0.8 \cdot 10^{-13}$ m$^{1/3}$, or a seeing of $0.''3$. It should remain clear that noise in MASS is *not a bias*, it must not to be subtracted from the measured layer strengths or seeing.

6.4 Optimization of the aperture geometry

The size of apertures in MASS was selected to match the Fresnel radii for turbulent layers at different altitudes. Now we can refine this choice and look for such aperture geometry that would lead to most accurate profile restoration. This can be done with the help of Eq. 13, under the approximation that input data are independent and the best least-squares restoration corresponds to the best separation of turbulent layers by MASS apertures. However, the problem of aperture optimization does not have a unique solution. First, the optimum geometry depends on the desired vertical resolution, i.e. the number and altitudes of pre-defined slabs. Secondly, the noise in MASS depends on the turbulence profile.

We selected five fixed layer altitudes at 1, 2, 4, 8, and 16 km. The noise was modeled as 2% of scintillation indices (except s_{AB} where it was 4%) for a fiducial profile with 0.6 of its energy at 1 km and the rest equally divided between 4 and 16 km. The wavelength of 450 nm and spectral bandwidth of 100 nm were assumed, close to real MASS parameters. For each trial aperture geometry the WFs and indices were found and then the noise of J_i was computed from Eq. 13. Maximum value of relative noise $r_i = \sigma_{Ji}/J_{\mathrm{tot}}$ was taken as a measure of restoration quality. We found that the best aperture diameters are 2, 3, 6, and 8.5 cm and that the maximum noise of $r = 0.1$ occurs at 4-km layer. Optimum aperture geometry only weakly depends on the input turbulence profile. Restoration quality is quite forgiving to the deviations from the optimum aperture ge-
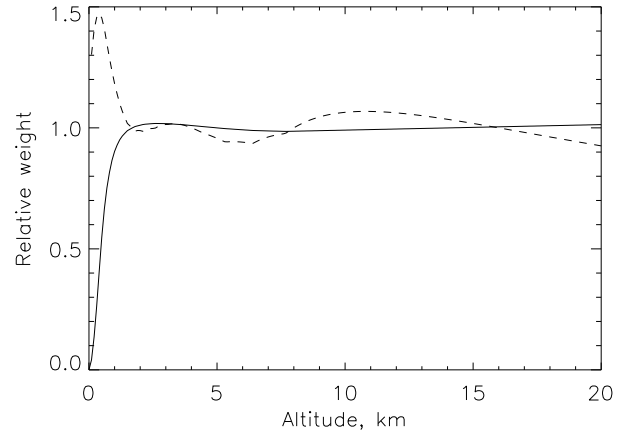
Figure 9. Ratio of the MASS weighting functions for free-atmosphere seeing $W_0(h)$ (full line) and isoplanatic angle $W_{5/3}(h)$ (dashed line) to the ideal h^0 and $h^{5/3}$ laws, respectively.

ometry; for the actual MASS apertures it is only marginally worse than for the optimal apertures.

7 DIRECT MEASUREMENT OF SEEING AND ISOPLANATIC ANGLE

Seeing is related to the integral of $C_n^2(h)$ over the whole atmosphere, J_{tot}. MASS is not sensitive to ground-layer turbulence (unless generalized mode is used), but it can measure the seeing produced by all higher layers which we call *free-atmosphere seeing*. The FWHM of long-exposure stellar image in a large telescope, ϵ, is the generally accepted seeing characteristics. The standard turbulence theory provides one-to-one correspondence between ϵ and the Fried parameter r_0, $\epsilon = 0.98\lambda/r_0$. The relation of r_0 to the turbulence integral J_{tot} is well known (Roddier 1981).

Free-atmosphere seeing at zenith is defined to be

$$\epsilon_f = 5.307\lambda^{-1/5} \left(\int_0^\infty C_n^2(h)W_0(h)\mathrm{d}h \right)^{3/5}, \tag{16}$$

where the function $W_0(h)$ determines which layers contribute to the seeing: it is equal to 1 at high altitudes and drops to zero at ground level. The integration is done over all altitudes, from the observatory level up. Free-atmosphere seeing is thus dependent on the somewhat arbitrary definition of $W_0(h)$. With $W_0(h) = 1$ everywhere we obtain the standard relation of seeing to the zeroth moment of turbulence profile J_{tot} (Roddier 1981). The constant $5.307 = 0.98 \cdot 0.432^{3/5} \cdot (2\pi)^{6/5}$.

Isoplanatic angle θ_0 characterizes the size of corrected field-of-view in adaptive optics (Fried 1982). It is related to the 5/3-rd moment of turbulence profile. Putting $W_{5/3}(h) = h^{5/3}$, the isoplanatic angle at zenith is

$$\theta_0 = 0.1334\ \lambda^{6/5} \left(\int C_n^2(h)W_{5/3}(h)\mathrm{d}h \right)^{-3/5}, \tag{17}$$

where $0.1334 = (2.91\ \pi^2)^{-3/5}$.

The turbulence moments can be obtained from SIs directly, without profile restoration. Each SI is an integral over altitude of C_n^2 multiplied by some WF. Thus, any linear combination of SIs corresponds to the linear combination of WFs. If it approximates
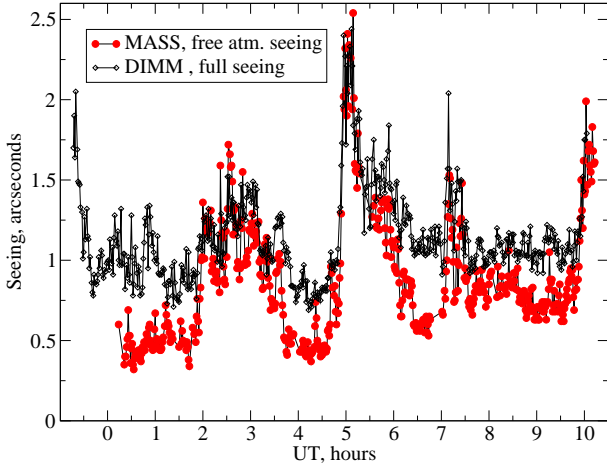
Figure 10. Comparison of the full atmospheric seeing as measured by the differential image motion monitor, DIMM (line with diamonds) and the free-atmosphere seeing measured by MASS (filled circles) on the night of March 27/28 2002. Strong turbulence layer at altitude around 1 km appeared sometimes and completely dominated the seeing, in which case DIMM and MASS measured the same seeing. Otherwise the seeing measured by DIMM is always worse than ϵ_f because it includes a large contribution of the ground layer which is not sensed by MASS.

the desired moment-generating weights W_0 and $W_{5/3}$, the moments can be estimated from linear combinations of indices. For example, in order to estimate ϵ_f we search such coefficients c_m^0 that

$$W_0(z) \approx \sum_{m=1}^{M} c_m^0 W_m(z). \tag{18}$$

Here we substitute altitude h with the propagation distance z. When ϵ_f and θ_0 are computed, they are transformed to viewing at zenith by multiplication by $(\cos\gamma)^{3/5}$ and $(\sec\gamma)^{8/5}$, respectively. However, the lower cutoff of the free-atmosphere seeing weight $W_0(h)$ does depend on γ: somewhat lower layers are included into ϵ_f estimate for non-zenith viewing.

To obtain c_m^0, we write Eq. 18 in matrix form for a discrete set of altitudes $\{z_i\}$ and solve for the vector c_m by singular value decomposition of the matrix $W_m(z_i)$. The same procedure applies for $W_{5/3}(h)$.

The coefficients c_m for moment estimation obtained by this procedure depend on the choice of altitude grid and the set of indices that enter into Eq. 18. Of course, we can use all measured indices and require the approximation to be as precise as possible. However, the coefficients thus obtained are large and of both positive and negative signs. In computation of moments the errors of index measurements would increase to the point that even negative moments can sometimes be obtained.

To avoid noise amplification, we restrict both the set of indices used for moment computation and the finesse of the altitude grid. For free-atmosphere seeing we take only the indices s_A, s_B, and s_{AB} and select the coarse altitude grid: 1, 2, 4, 8, 16 km. This results in a very reasonable $W_0(h)$ (Fig. 9) with the coefficients of -0.06, 0.09, and 1 for s_A, s_B, and s_{AB} respectively. Noise in the estimate of ϵ_f is dominated by the noise in s_{AB} (4% relative), permitting seeing measurements with a relative accuracy of 2.4%. Similar approximation for $W_{5/3}(h)$ is also shown in Fig. 9. The deviations from the ideal $h^{5/3}$ at low altitudes are not important because low altitudes are weighted by $h^{5/3}$. Actual approximations

used in data reduction are slightly different from those in Fig. 9, depending on software implementation details, spectral type of the star used, etc.

Moments are computed from the SIs measured every second. For a total 1-minute accumulation, the moments are averaged and their errors are estimated from the scatter of individual values in the same way as for the average indices (Eq. 7).

In Fig. 10 a comparison of ϵ_f with full seeing ϵ measured simultaneously on the same site is shown. Despite the fact that the two instruments, MASS and Differential Image Motion Monitor, use completely different principles (scintillation analysis and image motion, respectively), their results coincide when the dominating turbulent layers are in the free atmosphere (Tokovinin et al. 2003).

We compared ϵ_f computed directly from the moments with ϵ_f computed from the restored profiles and found that they agree to within 2%. This is not surprising, given that both are calculated from the same set of SIs. We found that ϵ_f from profiles is systematically larger that ϵ_f from moments when turbulence at low altitudes is present. This is explained by the specific altitude weighting: for profile restoration the sum of response functions has a 'hump' around 0.5 km (Fig. 5) where our $W_0(h)$ smoothly decays (Fig. 9).

8   CONCLUSIONS

The principle of TP measurement from SIs in concentric-ring apertures is presented, with detailed description of data-processing steps needed to convert the raw photon counts into altitudes and strengths of turbulent layers. This technique is based on photometry; the only calibration parameters needed for correct data interpretation are the sizes of apertures, spectral response of the instrument and the characteristics of photon counters. Examples of real data reductions are given.

MASS is an inexpensive instrument that uses only a small telescope. It is well adapted for TP monitoring at existing observatories and at new sites. We have started to use this technique for building an extensive database of TPs at several sites, e.g. (Tokovinin et al. 2003). When these data are complemented with meteorological information and 3D computer modeling of turbulence, a better understanding of the 'seeing' phenomenon will result, with important practical consequences for site selection. Another use of MASS will be to support the operation of adaptive-optics systems that can be enhanced or made more efficient if TP is known in real time.

APPENDIX A: DERIVATION OF EQUATIONS 5 AND 6

Here we derive the Eqs. 5,6. Let x_i be the individual photon counts in some aperture, B_x – average background flux in the same aperture. The scintillation index s_x can not be computed from its definition (1) by simply replacing true flux X with photon counts x_i because counts fluctuate even at constant flux owing to the random nature of photo-detection. The photon-noise variance is equal to the mean value $\overline{x}$ for an ideal detector. For real PMT it is $p\overline{x}$, where the

non-Poisson factor p can be slightly more than 1 for many reasons, e.g occasional after-pulses. Photon noise is independent from scintillation and must be subtracted from the measured variance. So, in order to obtain SI we compute the variance of photon counts $\rho_{xx,0}$ (Eq. 3), subtract photon noise and normalize by the square of mean stellar flux $\overline{x} - B_x$:

$$s_{x,1} = \frac{\rho_{xx,0} - P\overline{x}}{(\overline{x} - B_x)^2}. \tag{A1}$$

The notation $s_{x,1}$ reminds that the SI is computed for 1 ms sampling time and is not yet corrected to zero micro-exposure.

Photon noise in any two channels x and y is not correlated and does not distort the covariance $\rho_{xy,0}$. It follows from Eq. 2 that

$$s_{xy,1} = s_{x,1} + s_{y,1} - 2\frac{\rho_{xy,0}}{(\overline{x} - B_x)(\overline{y} - B_y)}. \tag{A2}$$

What remains is the extrapolation of indices to zero exposure time. This can be done by binning the data and computing the index for double micro-exposure $s_{x,2}$. The SI for zero exposure $s_{x,0}$ can then be estimated by linear interpolation

$$s_{x,0} = 2s_{x,1} - s_{x,2} \tag{A3}$$

which was shown to be a reasonable approximation (Tokovinin 2002). Such correction is really important for the differential SIs with the smallest MASS apertures, where 1 ms is not short enough to 'freeze' fast layers (for a 30 m/s wind speed the layer displacement is 3 cm, larger than the 2 cm aperture). For large apertures, the finite duration of micro-exposure is not important, although we still apply the correction.

Instead of actually binning the counts and repeating all calculations, we take advantage of pre-computed covariances with time lag. Let σ_2^2 be the variance of doubly-binned data, σ_1^2 – the variance of unbinned data, and $\rho_{xx,1}$ – the covariance with time lag 1. It can be shown easily that

$$\sigma_2^2 = 0.5(\sigma_1^2 - \rho_{xx,1}). \tag{A4}$$

The variance for zero exposure σ_0^2 is extrapolated as $\sigma_0^2 = 1.5\sigma_1^2 - 0.5\rho_1$. Now the transition from 1 ms indices as given by Eqs. A1,A2 to 0 ms indices (Eqs. 5,6) is straightforward.

APPENDIX B: FORMULA FOR WEIGHTING FUNCTIONS

Weighting functions for polychromatic scintillation were derived in (Tokovinin 2003). Here we give the computing formulae without derivation. The WF $W(z)$ is an integral over spatial frequency f:

$$W(z) = 9.62 \int_0^\infty f^{-8/3} A(f) S(z, f) df, \tag{B1}$$

where the factor $S(z, f)$ depends on the propagation range z, wavelength λ and the normalized spectral response $F(\lambda)$ (in photons per nm for a photon-counting detector):

$$S(z, f) = \left[\int \lambda^{-1} F(\lambda) \sin(\pi\lambda z f^2) d\lambda\right]^2. \tag{B2}$$

It can be seen that $S(z, f)$ is equal to the squared imaginary part of the Fourier Transform (FT) of $F(\lambda)/\lambda$. For monochromatic spectral response it reduces to the known $\lambda^{-2} \sin^2(\pi\lambda z f^2)$ term, whereas for real response we compute it by FT.

The aperture factor A is the square modulus of the FT of normalized aperture transmission function $P(\mathbf{x})$ or of their difference:

$$A(f) = |\tilde{P}(f)|^2 \qquad \text{for normal SI} \tag{B3}$$
$$A(f) = |\tilde{P}_1(f) - \tilde{P}_2(f)|^2 \qquad \text{for differential SI.} \tag{B4}$$

For a circular aperture of diameter D with a relative central obscuration ϵ

$$\tilde{P}(f) = \frac{1}{1 - \epsilon^2}\left[\frac{2J_1(\pi Df)}{\pi Df} - \epsilon^2\frac{2J_1(\epsilon\pi Df)}{\epsilon\pi Df}\right] \tag{B5}$$

For a special 'quasi-Gaussian' spectral response with FWHM Λ and central wavelength λ_0 the WF is

$$\begin{aligned} W(z) &= 9.62\lambda_0^{-2} \int_0^\infty df f^{-8/3} A(f) \exp(-1.780 z^2 f^4 \Lambda^2) \\ &\times \sin^2(\pi\lambda_0 z f^2). \end{aligned} \tag{B6}$$

REFERENCES

Fried D.L., 1982, J. Opt. Soc. Am., 72, 52

Fuchs A., Tallon M., Vernin J., 1998, PASP, 110, 86

Fuchs A., Vernin J., 1993, Final report on PARSCA 1992 and 1993 campaigns. Tech. Rep. VLT-TRE-UNI-17400-0010. ESO, Garching bei München, Germany

Kornilov V.G., Pogrosheva T.M., 1989, Astron. Zhourn. 66, 424

Kornilov V.G., Tokovinin A.A., 2001 Astron. Rep., 45, 395

Kornilov V., Tokovinin A., Voziakova O., Zaitsev A., Shatsky N., Sarazin M., 2002, Proc. SPIE, 4839, paper 102.

Le Louarn M., Hubin N., Sarazin M., Tokovinin A., 2000, MNRAS, 317, 535

Ochs G.R., Wang Ting-i, Lawrence R.S., Clifford S.F., 1976, Appl. Opt., 1976, 15, 2504

Peskoff A., 1968, J. Opt. Soc. Am., 58, 1032

Press W.H., Teukolsky S.A., Vetterling W.T., Flannery B.P., Numerical Recipes in C, Cambridge Univ. Press, Cambridge, UK, 1992

Rigaut F., in Vernet E., Ragazzoni R., Esposito S., Hubin N., eds, Beyond conventional adaptive optics, ESO Conf. Proc. 58, ESO, Garching bei München, Germany, 2002, 11

Roddier F., 1981, in Wolf E., ed., Progress in Optics, North-Holland, Amsterdam, 19, 281

Roddier F., ed., Adaptive optics in astronomy. Cambridge Univ. Press, Cambridge, UK, 1999

Tatarsky V.I., Wave propagation in a turbulent medium. Dover Publ. Inc., New York, 1961.

Tokovinin A., 1998, Astron. Lett., 24, 662

Tokovinin A., 2002, Appl. Opt., 41, 957

Tokovinin A., 2003, J. Opt. Soc. Am. (A), 20, 686

Tokovinin A., Kornilov V., 2002, in Astronomical Site Evaluation in the visible and Radio Range, Benkhaldoun Z., Muñoz-Tuñon C., Vernin J., eds, ASP Conf. Ser., 266, 104

Tokovinin A., Baumont S., Vasquez J., 2003, MNRAS, 340, 52